UNIVERSITY OF LEEDS

Proceedings Paper:
Kanoulas, D, Zhou, C orcid.org/0000-0002-6677-0855, Nguyen, A et al. (3 more authors) (2018) Vision-based foothold contact reasoning using curved surface patches. In: 2017 IEEE-RAS 17th International Conference on Humanoid Robotics (Humanoids). 2017 IEEE-RAS, 15-17 Nov 2017, Birmingham, UK. IEEE , pp. 121-128. ISBN 978-1-5386-4678-6

https://doi.org/10.1109/HUMANOIDS.2017.8239546

Vision-Based Foothold Contact Reasoning using Curved Surface Patches

Dimitrios Kanoulas, Chengxu Zhou, Anh Nguyen, Georgios Kanoulas
Darwin G. Caldwell, and Nikos G. Tsagarakis

***Abstract*— Reasoning about contacts between a legged robot's foot and the ground is a critical aspect of locomotion in natural terrains. This interaction becomes even more critical when the robot must move on rough surfaces. This paper presents a new visual contact analysis, based on curved patches that model local contact surfaces both on the sole of the robot's foot and in the terrain. The focus is on rigid, flat feet that represent the majority of the designs for current humanoids, but we also show how the introduced framework could be extended to other foot profiles, such as spherical feet. The footholds are localized visually in the environment's point cloud through a fast patch fitting process and a contact analysis between patches on the sole of the foot and in the surrounding environment. These patches aim to compose a spatial *patch map* for contact reasoning. We experimentally validate the introduced vision-based framework, using range data for rough terrain stepping demonstrations on the COMAN and WALK-MAN humanoids.**

I. INTRODUCTION

Since contacts between the sole of a robot's foot and the terrain on which it will stand need to be initially localized from a distance, visual perception plays a critical role in legged robot navigation. Modeling and reasoning about such contacts, especially for rough terrain, is one of the most challenging problems in legged locomotion [1]. The most recently developed humanoid robots use exteroceptive (e.g. stereo and lidar) perception to walk on flat surfaces with their soles in full contact with the environment [2], while rough terrain locomotion in natural environments, with potentially multiple sparse sole contact points, has been mainly handled with proprioceptive and low-level feedback control [3], [4]. At the same time, a significant amount of research has been done for quadruped locomotion based on visual feedback [5], due to their enhanced stability that comes from having multiple spherical feet, that can be considered as each having a point contact with the ground. However, a more generic perception system is required for contact shape modeling and reasoning between any robot's foot and rough surfaces in the environment. The purpose of this work is to provide such a generic contact reasoning framework.

In this paper, we develop a visual contact analysis system based on bounded curved patches, which model both the sole of the feet and local surfaces in the environment. The patch modeling and range data fitting method have been introduced in [6]. The primary, new contribution of this work is the presentation of a detailed mathematical contact reasoning between foot and environment patches. This enables the creation of a spatial contact *patch map* (Fig. 2-b). To represent the local surfaces of the environment we use 10 bounded curved patch types (Fig. 2-a), while we let the flat foot patches be rectangular planes (Fig. 3). This, is the most common foot design for bipedal robots. Consequently, contacts between foot soles and local areas on the terrain can be analysed as geometric contacts between different types of patches on and around the robot. The importance of this new framework, compared to other methods, is that it can also localize partial foot-surface contacts. This often occurs in natural environments, e.g. rocky (Fig. 1). The generic contact patch map can be used as an input in graph-based footstep path planning systems considering also other locomotion parameters [7], although we leave this for future work and focus on the visual contact analysis problem.

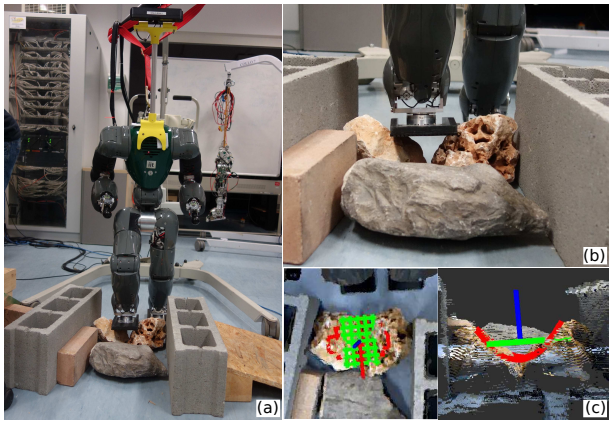

Fig. 1. (a) The humanoid robot COMAN stepping on a rocky surface using the introduced framework. (b) Foot contact close-up. (c) The environment fitted patch (red elliptic paraboloid) and the localized foot sole contact patch (green rectangular plane) from a top and side point of view.

The system has been implemented in the *Surface Patch Library* (SPL), with the code available on our website: `dkanou.github.io/projects/spl` [8]. Next we cover related work and review the curved patch modeling and fitting algorithms (Secs. I-A and II). We then give the contact representation details and the contact reasoning analysis (Secs. III and IV). Finally, we present experimental results on the COMAN [9] and WALK-MAN [10] bipeds using real range data (Sec. V). The introduced framework is an important step towards the implementation of a visual-driven path planner for humanoid locomotion on all terrains.

Dimitrios Kanoulas, Chengxu Zhou, Anh Nguyen, Darwin G. Caldwell, and Nikos G. Tsagarakis are with the Department of Advanced Robotics, Istituto Italiano di Tecnologia (IIT), Via Morego 30, 16163, Genova, Italy. {`Dimitrios.Kanoulas, Chengxu.Zhou, Anh.Nguyen, Darwin.Caldwell Nikos.Tsagarakis`}`@iit.it`, while Georgios Kanoulas is independent researcher. `gkanoulas@gmail.com`

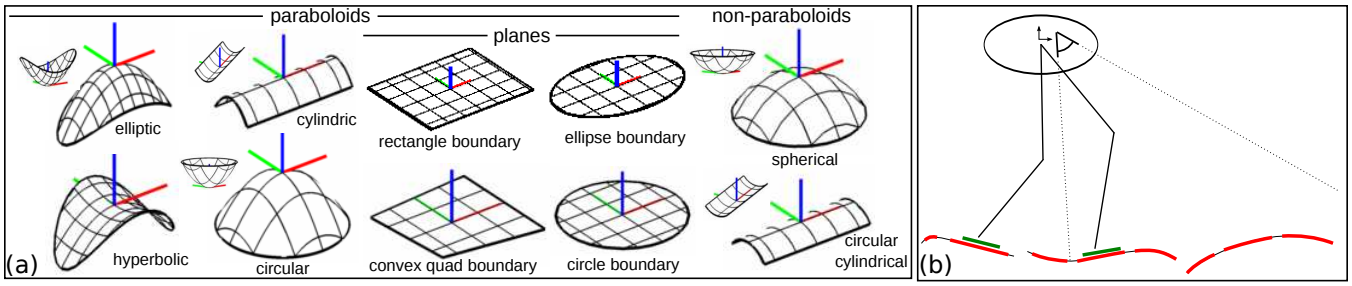

Fig. 2. (a) Ten bounded contact patch types. (b) A contact *patch map* instance composed by local environment (red) and feet sole (green) patches.

A. Related Work

Prior to the DARPA Robotics Challenge (DRC) 2015, there were only a few on-line vision-based methods for bipedal robot foot placement, especially for rough or uneven terrain locomotion. In [11], the humanoid HRP2 used stereo vision to detect and climb horizontal stairs, while in [12] the humanoid QRIO used range data to climb indoor sloping and elevated surfaces. 3D laser sensing was used in [13] to detect horizontal obstacles for climbing, while in [14] a similar concept was applied on HRP2. More recently in [15], [16], point cloud data were used in simulation to determine and avoid harsh footstep impacts on HRP2. Our goal differs in the fact that we search the environment for particular foot contacts that can be used for stable stepping. In [17] a footstep planning method was introduced for flat surface locomotion including stepping on obstacles for the NAO robot. A slightly different planner was introduced in [18] for flat terrain locomotion with real-time obstacle re-planning implemented on the NAO and HRP-4 robots. A multi-contact approach was demonstrated in simulation on HRP2 [19] using point cloud data for planar contact reasoning.

The challenges of the DRC generated increasing interesting work on footstep planning using range sensing for uneven terrain. In [2] an impressive stereo-based perception and optimization-based planning system was introduced for the humanoid robot ATLAS, while other teams, e.g. [20], mainly used graph-based planners for flat surfaces based on lidar measurements. The latter models were usually adjusted by human supervisors [7]. Most of the aforementioned works consider full foot contact with flat surfaces, usually by extracting planes in the environment. In this work, we, however, consider visual perception for foot contacts that are potentially partial and on both curved and flat surfaces. It is worth noting that in [21] a single point foot contact with the terrain was assumed in simulation for locomotion in unstructured environments without the use of vision.

On-line foot placement research for quadrupeds and hexapods has also a significant history in locomotion [22]–[24]. Recently, impressive control, planning, and perception systems have been introduced for full-size quadrupeds, such as the StarlETH [5] and the HyQ [25]. These types of robots usually assume point-like contacts with the environment, which differentiate them from the bipeds with respect to visual perception. However, we do introduce a generic framework that can be extended to also handle spherical foot types (Appendix I).

II. PATCH MODELING AND FITTING

Representing and geometrically reasoning about contacts between a robot's foot and local surfaces in the environment, using 3D visual perception, is considered a very challenging but necessary task in legged locomotion. In this work, we model contact surfaces with a set of ten bounded curved patches (Fig. 2) introduced in [6], from which eight are paraboloids and two are non-paraboloids. These patches can model both regular and irregular surfaces, on (i.e. the sole) and around (i.e. local terrain surfaces) the robot, with a compact and geometrically meaningful parametrization. Here we briefly review them, but we refer readers to the original paper for a detailed description. In our previous work these patches were used heuristically on a small-size biped for static single-foot placement [26]. In this paper, we present a more detailed and structured contact reasoning analysis for dynamic stepping that has been extended to non-flat surfaces.

Patches are modeled explicitly with a set of intrinsic and extrinsic parameters that represent their shape and pose, respectively. Each patch's dimensionality depends on its type and boundary. The intrinsic parameters represent up to two principle curvatures $\kappa_{x,y}$ and up to five boundary lengths and angles. Rotation and translation vectors ($\mathbf{r} \in \mathbb{R}^3$, $\mathbf{t} \in \mathbb{R}^3$) model the 6DoF pose of the patch local coordinate frame L in the world frame W.

Paraboloids

The general *paraboloid* surface is explicitly parametrized by its intrinsic principle curvatures $\mathbf{k} \triangleq [\kappa_x \ \kappa_y]^T$ in L, and the extrinsic rotation $\mathbf{r}$ and translation $\mathbf{t}$ vectors in W:

$$z = zl(x, y) = \frac{1}{2}\mathbf{u}^T \operatorname{diag}(\mathbf{k})\mathbf{u} \in \mathbb{R} \qquad (1)$$

where $(x, y, z) \in \mathbb{R}^3$ is a point on the patch in L and $\mathbf{u} = [x \ y] \in \mathbb{R}^2$ are its explicit parameters. Notice that a rigid body transformation between the local L and the world W frame using $\mathbf{r}$ and $\mathbf{t}$ is feasible [6].

The patch type is defined by its principal curvatures. Without loss of generality we will let $|\kappa_x| \leq |\kappa_y|$. If $\kappa_x \neq \kappa_y$ and the curvatures have equal signs then the patch is an *elliptic paraboloid*, while in case of opposite signs it is a *hyperbolic paraboloid*. If one curvature is zero it is a *cylindric paraboloid*, while if $\kappa_x = \kappa_y$ it is a *circular paraboloid*. In the special case that both curvatures are zero, the patch is a *plane*. The local $\hat{\mathbf{z}}_l$ patch axis is always pointing outwards and positive/negative curvatures identify concave/convex patch types, respectively.

Paraboloids Boundaries

We let each paraboloid type have a particular type of boundary, assuring symmetry properties. Elliptic and hyperbolic paraboloids are bounded with an *ellipse* in their local xy plane, parametrized by its radii $\mathbf{d}_e \triangleq [d_x \; d_y]^T$, while circular paraboloids with a *circle*, parametrized by its radius d_c such that $\mathbf{d}_e \triangleq [d_c \; d_c]^T$ and satisfies

$$0 \geq e(\mathbf{u}, \mathbf{d}_e) \triangleq \mathbf{u}^T \operatorname{diag}([1/d_x^2 \; 1/d_y^2])\mathbf{u} - 1. \quad (2)$$

Cylindric paraboloids are bounded with an *axis aligned rectangle*, parametrized by its half-widths $\mathbf{d}_r \triangleq [d_x \; d_y]^T$, which define its counter-clockwise vertices:

$$\mathbf{v}_1 \triangleq \mathbf{d}_r, \mathbf{v}_2 \triangleq [-d_x \; d_y]^T, \mathbf{v}_3 \triangleq -\mathbf{v}_1, \mathbf{v}_4 \triangleq -\mathbf{v}_2 \quad (3)$$

while the following condition should hold

$$0 \geq q(\mathbf{u}, \mathbf{v}_1, \mathbf{v}_2, \mathbf{v}_3, \mathbf{v}_4) \triangleq \quad (4)$$
$$\max(l(\mathbf{u}, \mathbf{v}_1, \mathbf{v}_2), l(\mathbf{u}, \mathbf{v}_2, \mathbf{v}_3), l(\mathbf{u}, \mathbf{v}_3, \mathbf{v}_4), l(\mathbf{u}, \mathbf{v}_4, \mathbf{v}_1))$$

with l being the implicit form for a 2D line given two points.

For the planar patches case, we allow four different boundaries: *ellipse, circle, rectangle, or general convex quadrilateral*. The *convex quadrilateral* is defined by the half-diagonal lengths and the half angle between the diagonals as $\mathbf{d}_q \triangleq [d_1 \; d_2 \; d_3 \; d_4 \; \gamma]^T$, while its vertices satisfy Eq. (4) and are defined as $\mathbf{v}_i \triangleq d_i[\cos\phi_i \;\; \sin\phi_i]^T$, with $\phi_1 \triangleq \gamma, \phi_2 \triangleq \pi - \gamma, \phi_3 \triangleq \pi + \gamma, \phi_4 \triangleq -\gamma$, and $0 < \gamma < \pi/2$.

Non-Paraboloids

We also let two non-paraboloids, i.e. upright hemispheres and circular half-cylinders, model common contact surfaces. We let $(x, y, z) \in \mathbb{R}^3$ be a point on the patch in L and $\mathbf{u} = [x \; y] \in \mathbb{R}^2$. The explicit parametrization in L for an *upright hemisphere* with curvature κ (i.e. radius $|1/\kappa|$) is:

$$z = zl(x, y) = (1/\kappa)\left(1 - \sqrt{1 - \kappa^2 \mathbf{u}^T \mathbf{u}}\right) \quad (5)$$

while its borders are circular with $\mathbf{d}_e \triangleq [d_c \; d_c]^T$, satisfying Eq. (2) and $|\kappa| d_c \leq 1$.

The explicit form for a *circular half-cylinder* in the local frame L is defined as:

$$z = zl(x, y) = (1/\kappa)\left(1 - \sqrt{1 - \kappa^2 \mathbf{u}^T Y \mathbf{u}}\right) \quad (6)$$

where $Y \triangleq [0 \; 1]^T [0 \; 1]$ and its borders are rectangular, satisfying Eq. (4) and $|\kappa| d_y \leq 1$.

A. Patch Fitting

Having defined the ten patch types and their boundary parametrization, we also introduced in [26] the framework to automatically fit and validate those patches to a set of point cloud neighborhoods in real-time, using a Levenberg-Marquardt based method. These either uniformly sample the space, or fit particular salient areas of the environment, depending on the task to complete. Here we don't focus on the fitting process itself, rather we assume that the contact reasoning begins when a set of patches has been fitted in the environment around the robot's foot. We let the size of the fitted environment patches be slightly bigger than the foot size, as will be explained in the next section.

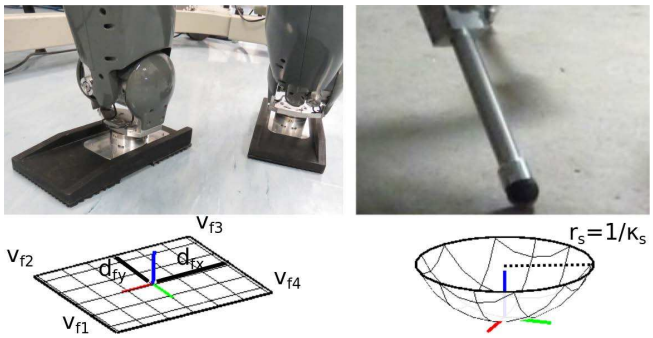

Fig. 3. Rectangular planar and circular half-spherical foot contact patches for legged robots, such as COMAN and HyQ.

III. PATCH CONTACT MODELING

In [26], we presented a simplified heuristic contact reasoning method between foot and environment patches for static foothold stepping using the Rapid Prototyped Biped (RPBP) robot. Its limitations lie in the fact that a library of environment patches associated with particular foot trajectories need to be created. Here we mathematically define a contact, and extend the above approach to automatic patch contact reasoning between the foot and the environment patches.

A. Foot Patch Modeling

Planar feet are a very common design among bipeds and thus we represent them with rectangular planar patches (Fig. 3). A flat foot patch p_f will be a plane with rectangle boundary, parametrized by its 6DoF pose ($\mathbf{r_f}$, $\mathbf{t_f}$) and its rectangle half-widths ($\mathbf{d}_{rf} = [d_{xf} \; d_{yf}]^T$) as described in Eqs. (1), (3), and (4), with $\kappa_x = \kappa_y = 0$ (Fig. 3-left).

B. Patch Contact Modeling

The contact between a foot (p_f) and an environment (p_e) patch will be parametrized by:

- a contact patch p_c, which has the same intrinsic parameters and type as the foot patch, but updated extrinsic parameters, i.e. its local frame in world coordinates.
- the set of N contact points $pt_{c_i} \in \mathbb{R}^3$, for $i \in [1, N]$ between p_c and p_e and the contact type, i.e. discrete points and continuous lines or surfaces.

The required contact type for stable stepping depends mainly on the planning and control methods that have been developed on each robotic platform. Usually, legged robots with four or more spherical feet require at least one contact point per foot [25], while bipeds with flat feet usually require at least three non-collinear contact points [15]. Only recently the impressive results in [4] showed that a contact line and in some cases a single contact point is enough for short time flat feet locomotion. We will analyse all the possible contact types between patches and let the corresponding robot planner use them accordingly. In our experiments we require at least three non-collinear contact points.

The original concept of the bounded curved patches was to let each one represent a foothold. Thus, the contact analysis will be done on this basis, even if some environment patches may overlap when they are fitted to a point cloud. First, we

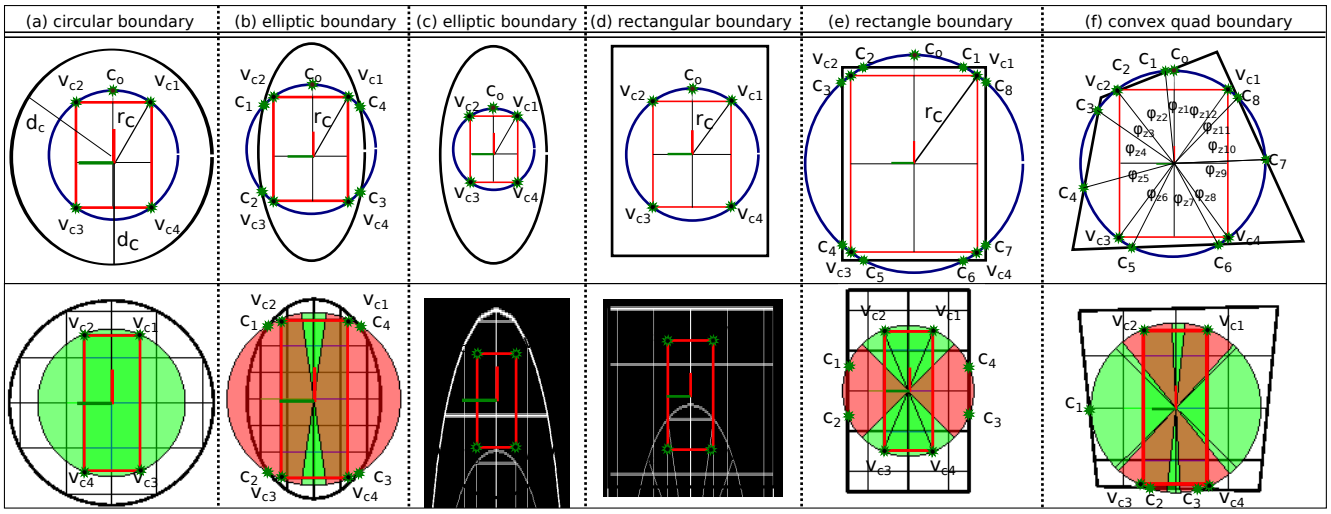

Fig. 4. The rotation analysis for a rectangular planar foot patch (red boundary) within each environment patch's boundary type (black boundary) in the xy-plane. $\mathbf{v_c}$'s are the vertices of the foot rectangular patch, r_c the radius of the foot patch's enclosing circle, and $\mathbf{c}$'s the intersection points between the enclosing circle and the environment patch boundary (if any). For the convex quad boundary (at the right part) the angle splits ϕ_z's are also visualized. In the bottom we provide some examples of valid (resp. invalid) angles in green (resp. red) after the 2D rotation analysis.

require the environment patch (p_e) boundary to be slightly bigger than the foot/contact patch's (p_c) one, by selecting the appropriate local fitting point cloud neighborhood radius. Secondly, we require the projection of p_c onto p_e's xy-local frame to be inside its 2D projected boundary. In this way there is no risk that the foot will make contact with unknown parts of the environment that are not represented by p_e's boundaries. Last, to also keep the symmetric properties of the patches, we constrain the contact patch's (p_c) origin to lie along the environment patch's (p_e) z-axis and translate/rotate only along/around it. Given that p_c's size is slightly smaller than p_e's one, this constraint does not affect the contact reasoning. Having defined the contact shape model, in the next section we present the patch contact case analysis.

IV. Patch Contact Reasoning

Given the foot patch (p_f) parametrization defined by the robot's physical foot size and shape, and a set of environment patches (p_e's) that fit to r-sized point cloud neighborhoods in the environment[1], the localization and parametrization of the contact patches (p_c's) for each environment patch (p_e) takes place in three steps:

1) p_f patch boundary containing check wrt p_e's one
2) p_f's rotation analysis around p_e's z-axis
3) p_f's contact points localization with p_e

These three steps identify and localize a contact, i.e. a contact patch and the contact points/type for all the possible rotational configurations of the foot patch around the environment patch's z-axis. The first two steps take place in the projected patches onto the p_e's local xy plane, while the last one is in the world coordinate frame.

A. Patch Boundary Containing Check

It is first required to check whether the foot patch fits inside the environment patch boundary, when both are projected onto p_e's local xy-plane. We call this the *containing criterion*. Without loss of generality, we assume that $d_x \geq d_y$ for all the patch boundaries and we let the *nominal pose* of the patches be the configuration where p_c's and p_e's origin and xy-axes co-align. For the convex quad case, we let the local xy-axis be originally arbitrary oriented.

For a *planar foot patch* p_f in the nominal pose, we ensure that its rectangle vertices, as defined in Eq. (3), satisfy the corresponding p_e's boundary constraints in Eq. (2) and (4). For environment patches with a convex quad boundary we heuristically let the foot patch rotate around the z-axis until all its points (if any) satisfy Eq. (4).

This process assures that a projected foot patch can be contained into an environment's patch boundary at their nominal pose. We set the initial contact patch p_c be the foot patch defined during this process. For those contact patches that pass this check we need to identify all the possible orientation angles around the z-axis such that the containing criterion remains true.

B. Contact Patch Rotation Analysis

There are only four types of boundaries in the patch type set that we introduced: elliptic, circular, rectangular, and convex quadrilateral. For each of them we will compute the valid counter-clockwise (ccw) rotation angles, ϕ_z, around the z-axis in the local frame L, such that the contact patch remains within the environment patch boundary. In the starting configuration, p_c and p_e are at the nominal pose, assuming that they passed the boundary containing check.

In the case of a *planar contact patch* with a rectangular boundary, whose vertices are $[\mathbf{v}_{c1}\ \mathbf{v}_{c2}\ \mathbf{v}_{c3}\ \mathbf{v}_{c4}]^T$), we propose a generic method to find the ϕ_z set. We first define an enclosing circle, centred at p_c's center, with radius $r_c = \sqrt{d_{xc}^2 + d_{yc}^2}$, where d_{xc} and d_{yc} are p_c's half-widths. Then we consider the following cases as illustrated in Fig. 4.

When the environment patch boundary is *circular* (Fig. 4-a) and the initial containing criterion holds ($r_c \leq d_c$), any

[1] r is the point cloud neighborhood size that a patch fits to and we refer readers to [26] for more details.

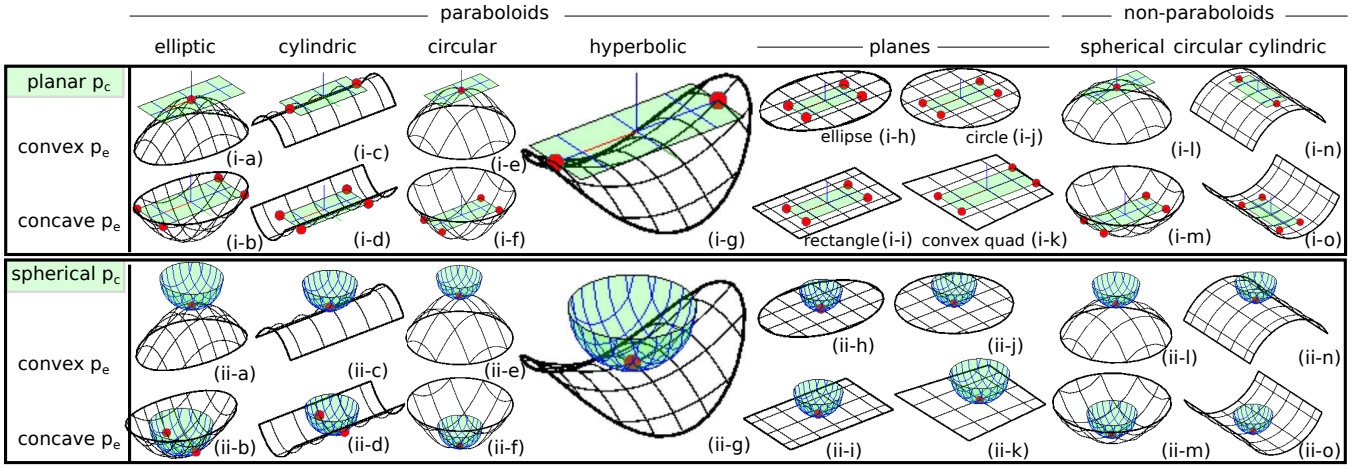

Fig. 5. The contact analysis in 3D between a foot patch (green planar on top and spherical in the bottom) for all the convex and concave environment patches. The red points are the contacts; in some cases they describe whole surface or segment/arc contacts (see the analysis in the text).

rotation around the z-axis is valid, resulting to $\phi_z = [0, 2\pi]$.

For the rest of the boundary types (*ellipse, rectangle, and convex quad*) we first compute the N intersection points $\{c_1, \ldots, c_N\}$ between p_e and the contact patch's r_c-radius enclosing circle (we do not consider tangent lines as intersecting). For the *elliptic* boundary there could be 0 or 4 intersecting points, while for the *rectangular* and *convex quad* boundaries there could be up to 2 intersecting points per line. We skip the mathematical analysis for finding these intersection points due to space limits, but we refer readers to find the details in our implementation. We enumerate the intersection points in a ccw order starting from the point which appears first in the circle after $\mathbf{v}_{c1}$. The interesting geometrical property of these intersection points is that they represent the order in which the contact patch vertices ($\mathbf{v}_{ci},\ i = 1, 2, 3, 4$) are alternating from being inside and outside p_e's boundary when p_c is rotating ccw. Each vertex $\mathbf{v}_{ci}$ first moves outside the boundary at the first intersecting point that appears when rotating ccw and moves inside again at the following point, and so on so forth. For instance, for the convex quad ccw rotation example in Fig. 4-f, $\mathbf{v}_{c1}$ moves outside p_e's boundary at intersection point c_1 and enters back in at c_2, and similarly for all the vertices. We split the circle into $N+5$ segments defined by $\{\mathbf{v}_{c1}, ..., \mathbf{v}_{c4}\}$, $\{c_1, ..., c_N\}$, and a point c_o in the intersection between the x-axis and the circle. Starting from c_o, each segment corresponds to an angle ϕ_{z_i}, for $i \in \{1, \cdots, (N+4)\}$. For each vertex $\mathbf{v}_{ci}$, $i \in \{1, 2, 3, 4\}$, we compute the segments that it remains inside the boundaries when p_c is rotated ccw, by alternating its status when a c_i point is met. We then need to find the ϕ_{z_i} set for which every vertex is inside the boundary. This is a collinear line segment overlapping problem, which becomes straightforward to be computed in the way we formed the problem above. In this way we extract all valid ϕ_{z_i} intervals for which p_c remains inside p_e's boundary.

Some examples of the process outcome appear at the bottom part of Fig. 4. Even though we presented a generic method for finding ϕ_{z_i}, in the implementation we take advantage of the symmetries that exist for rectangles and ellipses.

C. Contact Patch/Points Localization

Given a valid contact patch's 2D pose defined inside the environment patch boundary in the local coordinate frame L as described in the previous section, we need to identify: 1) the displacement δ of the contact patch (p_c) along the z-axis assuming that the origin is at the local p_e's axes, 2) the exact 3D contact points pt_c's in p_e's local axis, and 3) the type of contact (isolated points, line/arc segments, or full surfaces). These will uniquely determine the final contact.

Planar Foot Patch Contacts

For a rectangular planar foot contact patch, there are the following five environment patch type cases (Fig. 5-i):

- Convex (elliptic and circular) paraboloids and convex spherical non-paraboloids (Fig. 5-i-{a,e,l}). These environment patches have a single point of contact, which is p_e's origin, independently of the foot patch orientation. Thus, the displacement $\delta = 0$ and $pt_c = [0\ 0\ 0]$.
- Convex cylindric paraboloids and convex circular cylindric non-paraboloids (Fig. 5-i-{c,n}). These environment patches have a line segment contact along p_e's x-axis (smallest curvature). The displacement $\delta = 0$ and the two extreme points of the contact segment are:

$$pt_c = \pm[\frac{d_{yf}}{tan(\phi_z)}\ d_{yf}\ 0],\ \text{if } \theta < \phi_z < \pi - \theta$$
$$pt_c = \pm[d_{xf}\ d_{xf}tan(\phi_z)\ 0],\ \text{otherwise.}$$

  where $\phi_z = \phi_z\ mod(\pi)$ and $\theta = atan(\frac{d_{yf}}{d_{xf}})$.
- Concave (elliptic, cylindric, and circular) paraboloids and concave (spherical and circular cylindric) non-paraboloids (Fig. 5-i-{b,d,f,m,o}). These environment patches have either 2 or 4 contact points at p_c's vertices, depending on ϕ_z, i.e. p_c's orientation. Using Eq. (1) the displacement is $\delta = max(zl(\mathbf{v}_{fi}))$, for $i = \{1, 2, 3, 4\}$. The contact points are defined as $pt_c = [\mathbf{v}_{fxi}\ \mathbf{v}_{fyi}\ \delta]$, where $\mathbf{v}_{fxi}$ and $\mathbf{v}_{fyi}$ are the x and y components of the p_c's vertices whose z value equals δ.
- Planar (rectangular, elliptic, convex quad, and circular) paraboloids (Fig. 5-i-{h,i,j,k}). These environment

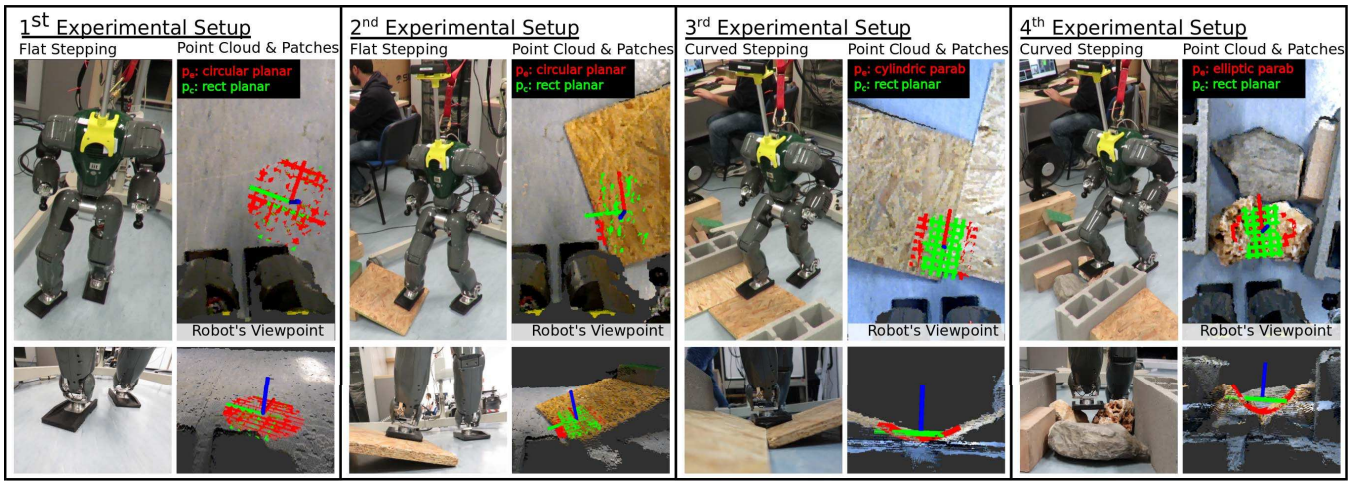

Fig. 6. Four experimental setups for COMAN stepping: on the left the robot and its foot in the final pose after stepping and on the right the fitted environment (red) and the foot contact (green) patches in the point cloud from the robot's viewpoint. Exp. 1: fits a circular planar patch oriented towards the robot. Exp. 2: fits a circular planar patch on an inclined (160° with the ground) flat surface. Exp. 3: fits cylindric/elliptic paraboloids and circular cylindric non-paraboloids between two 140° angled flat surfaces. Exp. 4: fits both paraboloids and non-paraboloids on a very rough rocky surface.

patches have their full surface in contact with p_e, with $\delta = 0$ and the vertices defining the convex contact surface are $pt_c = \mathbf{v}_{fi}$, $i = \{1, 2, 3, 4\}$.

- Hyperbolic paraboloid (Fig. 5-i-g). This environment patch is the most challenging one. To find the contact points we need to solve the following non-linear maximization problem with non-linear constraints:

$$max_{x,y} \frac{1}{2}(\kappa_x x^2 + \kappa_y y^2) \tag{7}$$

$$\text{s.t. } \frac{x^2}{d_x^2} + \frac{y^2}{d_y^2} - 1 \leq 0 \tag{8}$$

$$\text{and } q(\mathbf{u}, \mathbf{v}_1, \mathbf{v}_2, \mathbf{v}_3, \mathbf{v}_4) \leq 0 \tag{9}$$

where Eq. (7) defines p_e's paraboloid form, Eq. (8) p_e's elliptic boundary, and Eq. (9) p_c's rectangular boundary. This optimization problem localizes the hyperbolic paraboloid $(x, y, zl(x, y))$ points with the maximum z value in L, such that they are inside the foot and environment patch boundaries. We use the sequential quadratic programming (SQP) iterative method starting from the point with the maximum z-value on the ellipse boundary, which is along the paraboloid's x-axis. Practically, the algorithm was converging in less than 10 iterations.

The presented contact analysis for flat feet patches, can be extended to other foot sole types. In App. I we show the same analysis for round foot soles, which is common design for quadruped robot feet.

V. EXPERIMENTAL RESULTS

Having concluded the full contact analysis, we run a set of stepping experiments on the bipedal robots COMAN and WALK-MAN for regular and irregular terrains, using the introduced framework. Furthermore, we statistically analyse the patch fitting process to understand potential stepping failures for the contact patches due to visual inconsistencies.

A. Experimental Results on COMAN and WALK-MAN

COMAN and WALK-MAN are bipedal robots with 6DoF in each leg. They have planar 20×10cm and 32×15cm soles, correspondingly, and a mounted ASUS range sensor to provide point cloud data at 30Hz. Given that the autonomous seed selection and patch fitting method have been tested in our prior work, here we focus on evaluating successful robot stepping using the identified contact patches. The user selects manually a seed point in the robot's close proximity (i.e. the foot's workspace), around where a patch of size slightly bigger than the foot sole length fits (22cm for COMAN and 34cm for WALK-MAN). For this fitted environment patch the introduced contact analysis takes place and a contact foot patch is produced, oriented (x-axis) towards the robot's facing direction. The contact patch pose is sent to our gait pattern generator [9] for calculating the CoM and feet trajectories. Feed-forward joint angle compensation and an active compliant stabilizer [27] are used to eliminate the unexpected deflections (especially in the support leg's ankle and hip joint) and reduce the ground impact, due to swing foot's early landing resulted from the joints' compliance and backlashes.

We first ran 4 types of experiments on COMAN. Two to test our system for standard flat surfaces with full surface foot contact (Fig. 6, Exp. 1 and 2) and two for testing the ability to handle rough terrain with partial foot contact (Fig. 6, Exp. 3 and 4). We ran each experiment 5 times (20 times in total), and we noticed that for the planar environment patches there was never a failure in the stepping, while for the curved environment patches the robot failed to step stably on the surface 3 out of the 10 times. A reason for this, which is related to the visual contact localization, was due to incorrect patch fitting. In particular, there were cases where some 3D points were above the contact patch surface, e.g. the points at the green contact patch's sides of Exp. 4 in Fig. 6 (this may happen if the surface cannot geometrically be represented with a second degree paraboloid polynomial).

Contact Patch's Positive Residual (in mm)				
	1^{st} Exp.	2^{nd} Exp.	3^{rd} Exp.	4^{th} Exp.
Average Pos. Res. (1000 patches):	*3.17*mm		*11.7*mm	
Run 1	2.25mm	2.44mm	1.82mm	4.28mm
Run 2	2.72mm	1.75mm	1.63mm	**10.5mm**
Run 3	1.89mm	1.98mm	**5.22mm**	5.04mm
Run 4	2.98mm	3.09mm	4.43mm	**8.98mm**
Run 5	2.08mm	2.30mm	2.89mm	3.46mm

TABLE I
POSITIVE RESIDUALS FOR 5 STEPPING RUNS IN THE 4 EXPERIMENTAL SETUPS (SEE FIG 6) (IN BOLD THE UNSUCCESSFUL STEPPING).

In these cases the foot had early contact with the environment before it reaches its final reference pose and the robot fell, without the low level controller and stabilizer been able to handle the harsh impact. Some of these cases were handled in our prior work by running residual, coverage, and curvature evaluation, but even after this filtering there are still cases that may end up to unstable stepping.

B. Visual Analysis of the Experimental Results

To analyse the above failing cases we performed the following vision-only experiment (Table I). For the first two point clouds, for which all the stepping contacts were successful (Exp. 1 and 2) we fitted 1000 patches in the environment and we calculated the corresponding *positive residuals* (i.e. geometric residuals as introduced in [26], considering only the points above the contact patch surface, which cause early contacts with the environment). The mean positive patch residual (3.17mm) is a threshold indicator of potentially good contact patches, i.e. contacts become more risky as the positive residual grows bigger than this threshold. We ran the same experiment (1000 patches) for the last two point clouds (Exp. 3 and 4) that include rough surfaces and calculated the mean positive residuals (11.7mm). The amount of contact patches whose positive residual exceeded the 3.17mm threshold is 23%. We then ran the same experiment for all the contact patches during the 5 stepping runs per experimental setup, shown in Table. I. We verified that when the positive residual was diverging a lot from the threshold the robot was falling due to early contact with the environment (residuals: 5.22mm in the Exp. 3 and 10.5mm & 8.98mm in the Exp. 4). The positive residual justification can play a key role in selecting contact patches with bigger stepping success potential.

To show that the patch contact reasoning can be used for multi-step locomotion, we also ran a set of preliminary five-step locomotion experiments on WALK-MAN, for which one of the footholds was on rocky terrain (Fig. 7). The contact patches on the rock had in average a ~7.43mm positive residual, for which the stabilization control [27] allowed successful stepping on the rocks.

Last but not least, the time for fitting an environment patch and find the contact patch is in average ~1ms in the C++ implementation, for which only ~0.03ms is due to contact patch finding given the fitted environment patch. We invite the readers to watch the videos and try our implementation code under the SPL webpage: `http://dkanou.github.io/projects/spl`

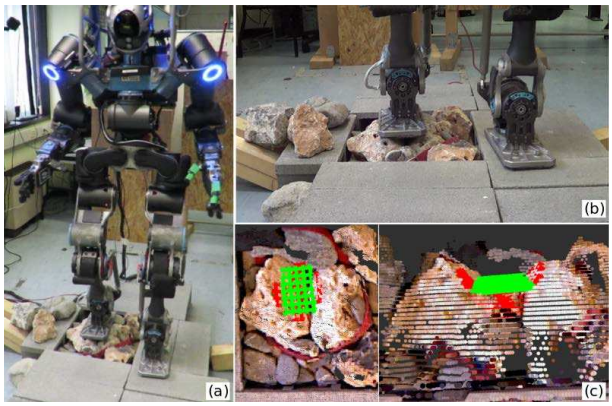

Fig. 7. (a) WALK-MAN performing 5-step locomotion: the second step on a rocky surface and the rest on flat. (b) Foot contact close-up. (c) The environment fitted patch (red elliptic paraboloid) and the localized foot sole contact patch (green rectangular plane) from a top and side point of view.

VI. CONCLUSIONS AND FUTURE WORKS

In this paper, we presented a framework for contact analysis between a planar foot sole and the environment, based on bounded curved contact patches. Our real-time system takes as input point cloud data in 30Hz from a range sensor and calculates a set of possible contact patches related to the fitted environment ones. We ran the framework on different scenarios on the COMAN and WALK-MAN bipeds and analysed the successful stepping with respect to the detected contact patches. We also showed how the contact theory can be extended to other foot types, such as spherical ones. The current work builds on and improves the heuristic methodologies that were used before for completing similar stepping experiments [26].

A next step is to integrate impedance control in order to allow a more stable stepping even when patches do not perfectly fit in the environment. Furthermore, an improved patch fitting algorithm needs to be studied, where there are no points above the contact surfaces. In addition, the experimental verification of the positive residual on the robot needs to be analysed. Our goal is to be able to integrate this framework in a patch-based path planner for walking into rocky terrain, using SLAM.

ACKNOWLEDGEMENT

This work is supported by the WALK-MAN & CogIMon (grant agreements no 611832 & 644727) EU projects. The authors would like to thank Enrico Mingo Hoffman and Luca Muratore for their valuable help during the experiments.

APPENDIX I

Here we show an extension of the contact reasoning analysis to a different foot type, i.e. round sole, which is among the most common feet designs on quadruped robots.

Foot Patch/Contact Modeling. We let a half-spherical foot patch p_s be a concave half-spherical patch with circular boundary, parametrized by its 6DoF pose ($\mathbf{r_s}$, $\mathbf{t_s}$) and its radius $d_s = 1/\kappa_s$ as described in Eqs. (2) and (5) (Fig. 3-right). The patch contact modeling is the same as described in Sec. III-B.

Patch Boundary Containing Check. For p_s we just need to assure that its circle radius d_s is smaller than p_e's circle radius d_c (for circular boundary), the minimum ellipse radius d_y (for elliptic boundary), the minimum rectangle axis half-width d_y (for rectangular boundary), or the minimum perpendicular distance from the convex quad's sides, defined as $\left|det(v_{(i+1)\%4} - v_{i\%4}, v_{i\%4})\right| / \left\|v_{(i+1)\%4} - v_{i\%4}\right\|$, for $i \in \{1, 2, 3, 4\}$ (for convex quad boundary).

Contact Patch Rotation Analysis. For p_s, it is straightforward that as long as the containing criterion holds for the initial poses, the contact patch can rotate freely around the local z-axis, resulting to $\phi_z = [0, 2\pi]$.

Half-Spherical Foot Patch Contacts. For p_s, there are the following four environment patch type cases (Fig. 5-ii):

- Convex (elliptic, cylindric, and circular) paraboloids, planar (rectangular, elliptic, convex quad, and circular) paraboloids, and convex (spherical and circular) cylindric non-paraboloids (Fig. 5-ii-{a,c,e,h,i,j,k,l,n}). These environment patches have a single point of contact, which is p_e's origin. Thus, the displacement $\delta = 0$ and $pt_c = [0\ 0\ 0]$.
- Concave spherical non-paraboloids (Fig. 5-ii-m). These environment patches may have either 1 point of contact (the origin of the environment patch p_e) when p_c's radius r_s is smaller than p_e's radius $1/\kappa$ or the full surface when $r_s = 1/\kappa$. In the former case the displacement $\delta = 0$ and $pt_c = [0\ 0\ 0]$.
- Concave circular cylindric non-paraboloids (Fig. 5-ii-o). These environment patches may have either 1 point of contact (the origin of the environment patch p_e) when p_c's radius r_s is smaller than p_e's radius $1/\kappa$ or its whole circle arc along p_e's y-axis, when $r_s = 1/\kappa$. In the former case the displacement $\delta = 0$ and $pt_c = [0\ 0\ 0]$. In the later case the displacement is also $\delta = 0$, while $pt_c = [0\ \pm d_y\ zl(\pm dy, 0)]$.
- Concave (elliptic, cylindric, circular, and hyperbolic) paraboloids (Fig. 5-ii-{b,d,f,g}). These environment patches may either have 1 or 2 points of contact. Assuming as before, without loss of generality, that the smallest curvature is along the x-axis ($\kappa_x \leq \kappa_y$), the contact analysis is done in the yz-plane. In Eqs. (1) and (5) we set $x = 0$ and in Eq. (5) z to be $z + \delta$:

$$z = \frac{1}{2}\kappa_y y^2 \quad \text{and} \quad y^2 + (z - (\frac{1}{\kappa} + \delta))^2 = \frac{1}{\kappa^2} \quad (10)$$

To find the two contact points, we require the solution of the above system to have a double real root. Skipping the calculations, it is straightforward to verify that the displacement is:

$$\delta = (\kappa - \kappa_y)^2/(2\kappa^2\kappa_y) \quad (11)$$

The two contact points are $pt_c = [0\ \pm 2\frac{|\delta|}{\kappa_x}\ \delta]$. If the above system has only one real solution, then there is only one contact point at the origin, with $\delta = 0$.

REFERENCES

[1] S. Kajita and T. Sugihara, "Humanoid Robots in the Future," *Advanced Robotics*, vol. 23, pp. 1527–1531, 2009.

[2] M. Fallon *et al.*, "Continuous Humanoid Locomotion over Uneven Terrain using Stereo Fusion," in *IEEE-RAS Humanoids*, 2015.

[3] C. Knabe *et al.*, "Designing for Compliance: ESCHER, Team VALORs Compliant Biped," *Journal of Field Robotics (JFR)*, 2016.

[4] G. Wiedebach, S. Bertrand, T. Wu, L. Fiorio, S. McCrory, R. Griffin, F. Nori, and J. Pratt, "Walking on Partial Footholds Including Line Contacts with the Humanoid Robot ATLAS," in *IEEE-RAS 16th Int. Conf. on Humanoid Robots (Humanoids)*, 2016, pp. 1312–1319.

[5] M. Wermelinger, P. Fankhauser, R. Diethelm, P. Krusi, R. Siegwart, and M. Hutter, "Navigation Planning for Legged Robots in Challenging Terrain," in *IEEE/RSJ IROS*, 2016, pp. 1184–1189.

[6] M. Vona and D. Kanoulas, "Curved Surface Contact Patches with Quantified Uncertainty," in *IEEE/RSJ IROS*, 2011, pp. 1439–1446.

[7] A. Stumpf, S. Kohlbrecher, D. Conner, and O. von Stryk, "Supervised Footstep Planning for Humanoid Robots in Rough Terrain Tasks using a Black Box Walking Controller," in *IEEE-RAS International Conference on Humanoid Robots (Humanoids)*, 2014, pp. 287–294.

[8] D. Kanoulas and M. Vona, "The Surface Patch Library (SPL)," in *IEEE ICRA Workshop*, 2014, dkanou.github.io/projects/spl/.

[9] C. Zhou, X. Wang, Z. Li, and N. Tsagarakis, "Overview of Gait Synthesis for the Humanoid COMAN," *Journal of Bionic Engineering*, vol. 14, no. 1, pp. 15–25, 2017.

[10] N. G. Tsagarakis *et al.*, "WALK-MAN: A High Performance Humanoid Platform for Realistic Environments," *JFR*, 2017.

[11] K. Okada, T. Ogura, A. Haneda, and M. Inaba, "Autonomous 3D Walking System for a Humanoid Robot Based on Visual Step Recognition and 3D Foot Step Planner," in *IEEE ICRA*, 2005, pp. 623–628.

[12] J.-S. Gutmann, M. Fukuchi, and M. Fujita, "3D Perception and Environment Map Generation for Humanoid Robot Navigation," *The Int. J. of Robotics Research*, vol. 27, no. 10, pp. 1117–1134, 2008.

[13] J. Chestnutt, Y. Takaoka, K. Suga, K. Nishiwaki, J. Kuffner, and S. Kagami, "Biped Navigation in Rough Environments Using On-board Sensing," in *IEEE/RSJ IROS*, 2009, pp. 3543–3548.

[14] K. Nishiwaki, J. Chestnutt, and S. Kagami, "Autonomous Navigation of a Humanoid Robot over Unknown Rough Terrain using a Laser Range Sensor," *IJRR*, vol. 31, no. 11, pp. 1251–1262, 2012.

[15] O. E. Ramos, M. García, N. Mansard, O. Stasse, J.-B. Hayet, and P. Souères, "Towards Reactive Vision-Guided Walking on Rough Terrain: An Inverse-Dynamics Based Approach," in *Workshop on Visual Navigation for Humanoid Robots (IEEE ICRA)*, 2013.

[16] N. Kita, M. Morisawa, and F. Kanehiro, "Foot Landing State Estimation from Point Cloud at a Landing Place," in *13th IEEE-RAS Humanoids*, 2013, pp. 252–259.

[17] D. Maier, C. Lutz, and M. Bennewitz, "Integrated Perception, Mapping, and Footstep Planning for Humanoid Navigation Among 3D Obstacles," in *IEEE/RSJ IROS*, 2013, pp. 2658–2664.

[18] P. Karkowski and M. Bennewitz, "Real-time Footstep Planning using a Geometric Approach," in *IEEE ICRA*, May 2016, pp. 1782–1787.

[19] S. Brossette, J. Vaillant, F. Keith, A. Escande, and A. Kheddar, "Point-Cloud Multi-Contact Planning for Humanoids: Preliminary Results," in *CISRAM*, vol. 1, 2013, p. 6.

[20] S. Kohlbrecher *et al.*, "Human-Robot Teaming for Rescue Missions: Team ViGIRs Approach to the 2013 DARPA Robotics Challenge Trials," 2014.

[21] O. Khatib and S.-Y. Chung, "SupraPeds: Humanoid Contact-Supported Locomotion for 3D Unstructured Environments," in *IEEE Int. Conf. on Robotics and Automation (ICRA)*, 2014, pp. 2319–2325.

[22] C. Plagemann, S. Mischke, S. Prentice, K. Kersting, N. Roy, and W. Burgard, "A Bayesian Regression Approach to Terrain Mapping and an Application to Legged Robot Locomotion," *Journal of Field Robotics*, vol. 26, no. 10, pp. 789–811, Oct. 2009.

[23] J. Z. Kolter, Y. Kim, and A. Y. Ng, "Stereo Vision and Terrain Modeling for Quadruped Robots," in *IEEE International Conference on Robotics and Automation (ICRA)*, 2009, pp. 3894–3901.

[24] M. Kalakrishnan, J. Buchli, P. Pastor, M. Mistry, and S. Schaal, "Learning, Planning, and Control for Quadruped Locomotion over Challenging Terrain," *IJRR*, no. 2, pp. 236–258, 2010.

[25] C. Mastalli, I. Havoutis, A. W. Winkler, D. G. Caldwell, and C. Semini, "On-line and On-board Planning and Perception for Quadrupedal Locomotion," in *IEEE TePRA*, 2015.

[26] D. Kanoulas, "Curved Surface Patches for Rough Terrain Perception," Ph.D. dissertation, CCIS, Northeastern University, August 2014.

[27] C. Zhou, Z. Li, X. Wang, N. Tsagarakis, and D. Caldwell, "Stabilization of Bipedal Walking Based on Compliance Control," *Autonomous Robots*, vol. 40, pp. 1041–1057, 2016.